Proceedings, 7th African Rift Geothermal Conference
Kigali, Rwanda 31st October – 2nd November 2018

Imaging Resistivity Structures of High-Enthalpy Geothermal Systems Using Magnetotelluric Method: A case study of Aluto-Langano geothermal field in Ethiopia

Cherkose Biruk Abera[1], Hideki Mizunaga[2] and F. Samrock[3]

[1]Geological Survey of Ethiopia, 2302, Addis Ababa, Ethiopia
[2]Department of Earth Resources Engineering, Faculty of Engineering, Kyushu University, Japan
[3]Institute of Geophysics, ETH Zurich, Switzerland

birukabera39@yahoo.com

Keywords

Magnetotelluric method, high-enthalpy, geothermal system, resistivity

ABSTRACT

Resistivity imaging using magnetotelluric (MT) method in high-enthalpy geothermal systems is an effective tool to identify conductive clay layers that cover the geothermal systems and to detect a potential reservoir. In this paper, we use MT data from Aluto-Langano geothermal field, a high-enthalpy geothermal field in Ethiopia with the objective of constructing a 3-D resistivity model of the subsurface to better understand the hydrothermal system of the area by correlating it with geology, alteration information from wells and a conceptual model of a high-enthalpy field. In particular, identifying the low resistivity zone associated with clay alteration zones (the cap rock) and delineating potential reservoir are the main tasks in this study. The result of the 3-D inversion identifies three main resistivity structures: a high-resistivity layer associate with unaltered volcanic rocks at shallow depths, a low-resistivity layer related to argillic alteration clay products, predominantly smectite and a gradually increasing high resistivity region at greater depths related to the formation of high-temperature alteration minerals such as chlorite and epidote. The recovered resistivity model corresponds very well with the conceptual model for high-enthalpy volcanic geothermal systems where an increase in resistivity below a highly conductive surficial layer (clay cap), reflect an increase in temperature with depth. This is a common signature of high-temperature geothermal systems.

1. Introduction

Investigating electrical resistivity of the subsurface in a high-enthalpy geothermal areas is a powerful prospecting method to understand structures related to the geothermal resource. Resistivity is directly related to parameters that characterize the geothermal reservoir, such as temperature, alteration, salinity and porosity (permeability) (Hersir and Björnsson, 1991). Electromagnetic methods, particularly MT is a commonly applied geophysical technique to map resistivity distribution in geothermal areas as it can image subsurface resistivity distribution easily down to depths of several kilometers. It is an effective tool to identify conductive clay layers that cover the geothermal systems and to detect a potential reservoir.

High-enthalpy hydrothermal systems have temperatures exceeding 150 ^{0}C and are made of high permeable regions confined by low permeability strata, cap rock (Munoz, 2014, Samrock et al., 2015) (Figure 1). The low permeable confining cap is produced by prolonged reactions of the rocks with the thermal fluids, which produce a clay alteration layer over a temperature range from under 100 ^{0}C to over 200 ^{0}C (Caldwell et al. 1986; Munoz 2014). Very conductive clay mineral, smectite is formed between 70 ^{0}C to 150 ^{0}C. Illite and chlorite become interlayered with smectite, forming a mixed layer over a temperature range from 150 ^{0}C to over 220 ^{0}C. Chlorite and epidote are the main alteration minerals at temperature over 220 ^{0}C. The resistivity increases gradually below the conductive layer at higher temperatures (> 200 ^{0}C) due to the formation of resistive minerals such as chlorite and epidote. Therefore, an increase in resistivity below a highly conductive surficial layer (clay cap), reflecting an increase in temperature with depth, is a common signature of high-temperature geothermal systems (Munoz 2014).

The conceptual model of a high-enthalpy geothermal systems constructed by Johnston et al., 1992 and Cumming and Mackie, 2007 describes the temperature pattern, alteration zones and resistivity distribution (Figure 1 and Figure 11B). Hydrothermally unaltered rocks at shallow depths result in high-resistivity layer (> 100 Ωm). In this region, the temperature is below 70 ^{0}C and alteration is minimum. Beneath the unaltered surface layer, a conductive layer in the Argillic alteration zone (70 - 200 ^{0}C) is mainly attributed to the presence of conductive clay alteration products, especially smectite. Generally, illite and smectite in argillic alteration zone characterized by low resistivity signatures below 10 Ωm. High temperature alteration minerals, chlorite and epidote at deeper depths beneath the conductive layer show relatively high resistivity (10 – 60 Ωm) in the propylitic alteration zone (Johnston et al., 1992; Pellerin et al. 1996; Cumming and Mackie 2007; Munoz 2014; Samrock et al., 2015; Cherkose and Mizunaga, 2018).

In this paper, we use data from two previous MT studies collected from 86 sites at Aluto-Langano geothermal field, a high-enthalpy geothermal field in Ethiopia (Figure 2). These data were acquired from surveys conducted in 2009 and 2012 by West Japan Engineering Consultants, Inc. (Ernst and Young et al., 2010; Cherkose and Mizunaga, 2018) and by a team of scientists from ETH Zurich, Addis Ababa University and the Geological Survey of Ethiopia (Samrock et al., 2015), respectively.

The objective of this study is to detect promising zones for geothermal development by studying the subsurface resistivity distribution obtained from the two MT survey results. In high-enthalpy geothermal systems, investigating subsurface resistivity distribution is vital to understand the geological structures related to geothermal resources and to determine the locations of the production and reinjection wells. The goal of this study is to construct a 3-D resistivity distribution model of the Aluto-Langano geothermal field to better understand the hydrothermal system and to contribute to the geothermal exploration in the area for further development.

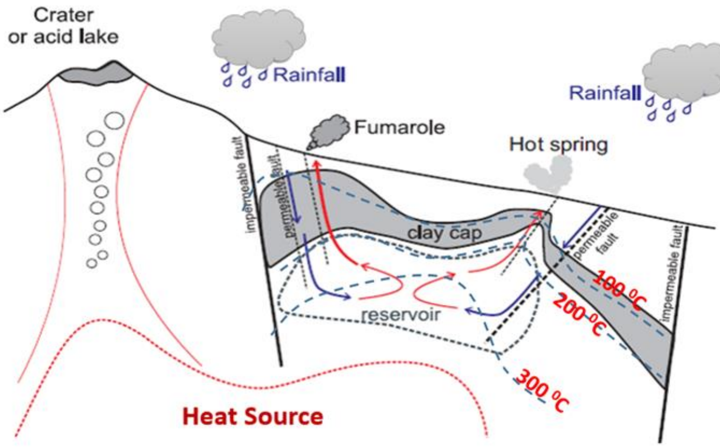

Figure 1: A conceptual model of a high-enthalpy geothermal system (Modified from Johnston et al., 1992; Pellerin et al. 1996; Cumming and Mackie, 2007; Munoz 2014; Niasari, 2015; Samrock et al., 2015; Cherkose and Mizunaga, 2018).

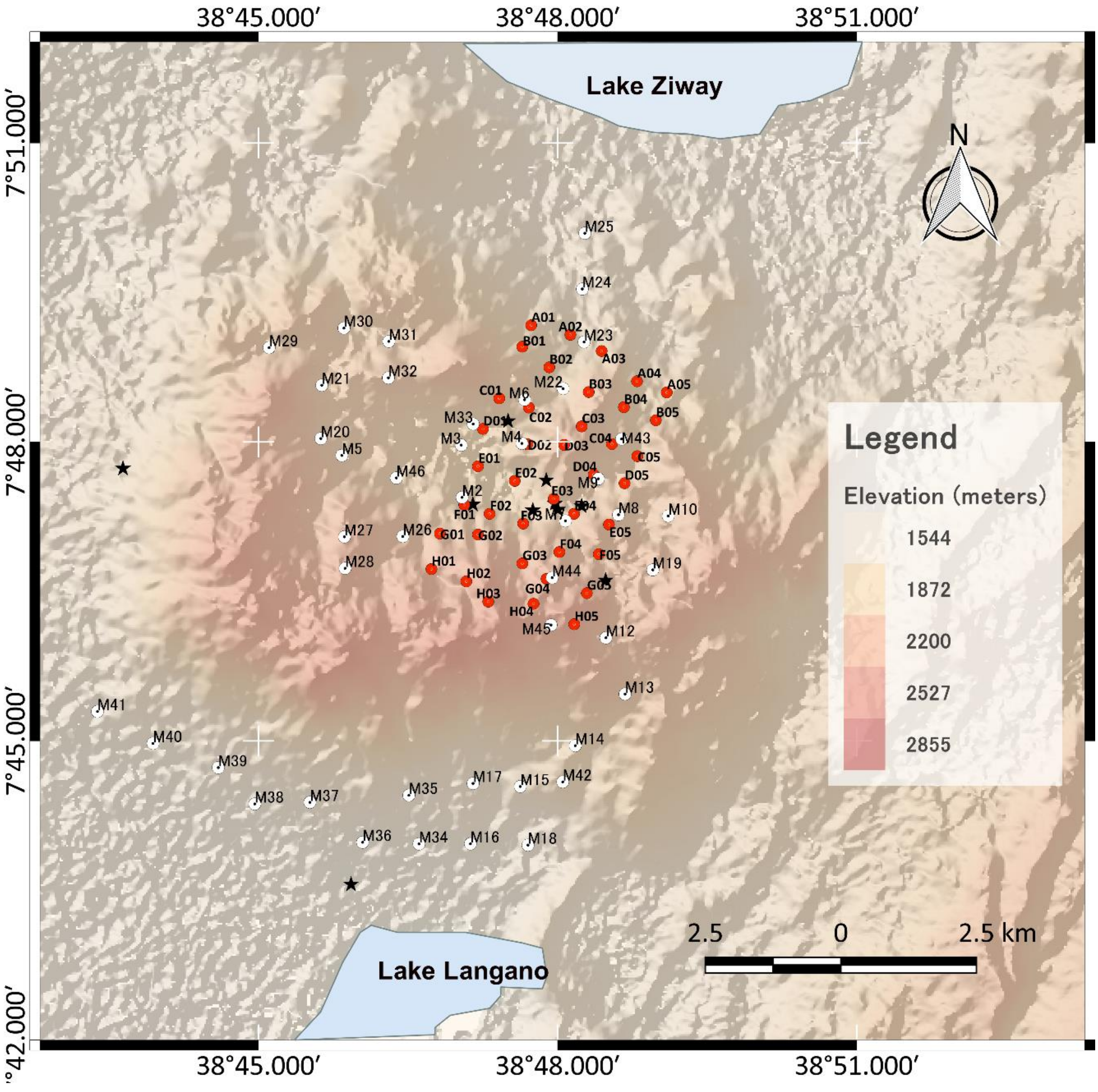

Figure 2: Location map of Aluto-Langano geothermal field. The white and the red dots denote location of MT stations from ETH 2012 survey and WestJEC 2009 survey, respectively. The black stars indicate deep geothermal wells.

2. MT Surveying in Aluto-Langano Geothermal Field

Aluto-Langano geothermal field (Figure 2) is located in the Central Main Ethiopian Rift (CMER) system close to the eastern escarpment of the rift along the NNE-SSW fault system, Wonji Fault Belt (WFB), enclosed by lake Ziway in the north and lake Langano in the south. Two deep geothermal wells, LA-9D and LA-10D finished in 2015 and eight wells (LA1- LA8) drilled between 1981-1985 with a maximum depth of 2500m indicated the existence of a high-enthalpy geothermal system with temperatures greater than 300 ^{0}C (Gebregzabher, 1986; Gianelli and Teklemariam, 1993; Cherkose and Mizunaga, 2018). Hydrothermal manifestation in the Aluto-Langano include hot springs, fumaroles, hot and warm ground as shown in Figure 3 (Abebe et al., 2016; Hutchison et al., 2016). The first geothermal power plant in Ethiopia began operation in this area in May,1998. A combined steam and binary cycle power plant with 7.2 MWe was constructed as a pilot project. Currently, expansion work of the power plant is underway to increase the production to 70 MWe.

The major outcropping rocks in Aluto-Langano geothermal field include volcanic and sedimentary units (Figure 3). The Tertiary ignimbrite units are the oldest rocks, outcropping on the eastern escarpment in the area. The Boffa basalt outcropping east, northeast and south of Aluto overlain the ignimbrite. Above the Boffa basalt, lacustrine sediments observed from the geothermal drillings below the pyroclastic and lava flows. The volcanic products of Aluto consist of a complex succession of ash-low tuff, silicic lithic tuff breccias, silicic domes and pumice flows lie either on top of the lake sediments or directly on the Boffa basalt (Gianelli and Teklemariam, 1993; Cherkose and Mizunaga, 2018).

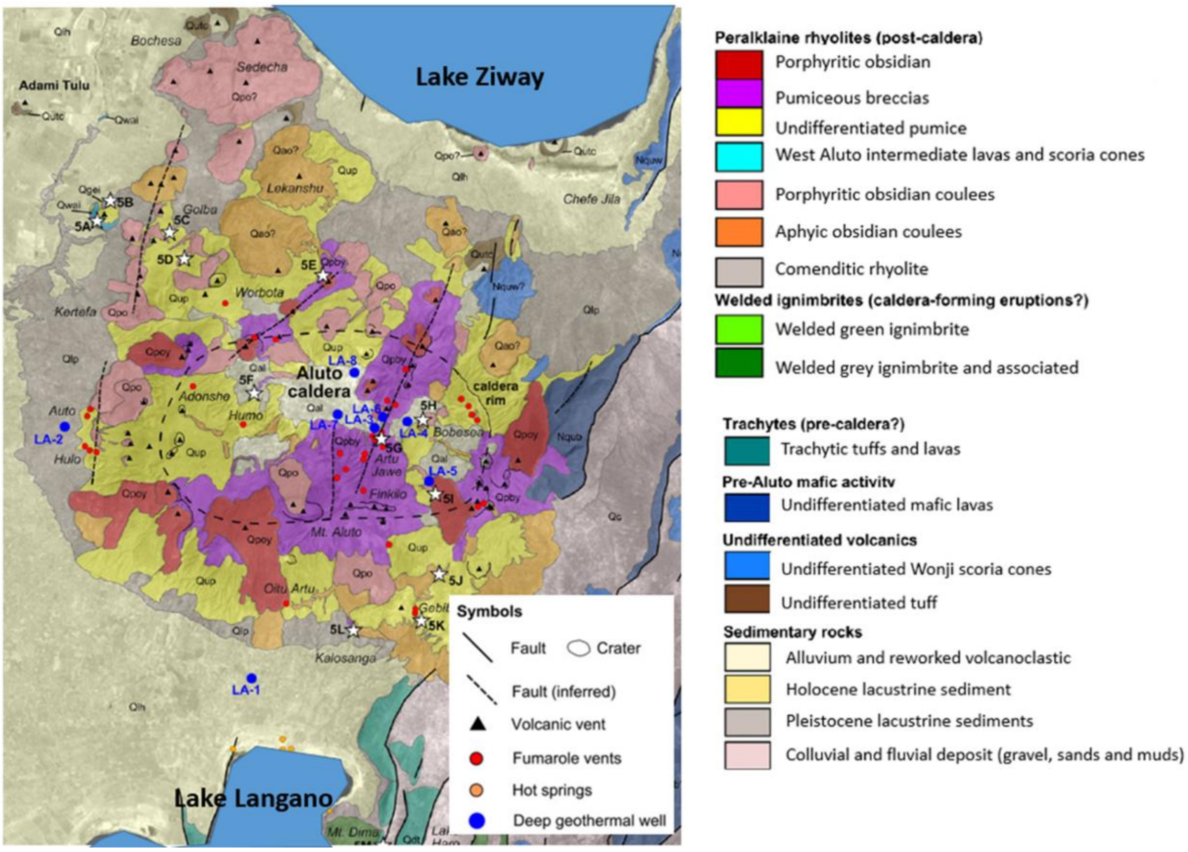

Figure 3: Surface geology of the Aluto-Langano geothermal field. (Redrawn from Hutchison et al., 2016). The blue dotes represent deep wells and red and orange dots indicate the locations of fumaroles and hot springs, respectively. The broken black lines indicate the fault systems in the study area.

3.1 Phase Tensor Analysis

The phase tensor is a practical tool to easily get information about the dimensionality of the regional structure. Calculation of the phase tensor requires no assumption about the dimensionality of the underlying conductivity distribution and is applicable where the regional structure is 3-D. The phase tensor $\boldsymbol{\Phi}$ is defined as the ratio of the real ($\boldsymbol{X}$) and imaginary parts ($\boldsymbol{Y}$) of the complex impedance tensor, $\mathbf{Z}$.

$$\boldsymbol{\Phi} = \boldsymbol{Y}/\boldsymbol{X}, \tag{1}$$

where

$$\mathbf{Z} = \boldsymbol{X} + i\boldsymbol{Y}, \tag{2}$$

The phase tensor can be depicted graphically by an ellipse, which consists of minimum (Φ_{min}) and maximum (Φ_{max}) principal axes, and skew angle (β) (Figure 4). The skew angle value is commonly displayed as colour filling of the ellipses in phase tensor maps. The phase tensor can be expressed in terms of Φ_{min}, Φ_{max}, α and β as follows:

$$\boldsymbol{\Phi} = \boldsymbol{R}^{\boldsymbol{T}}(\alpha - \beta)\begin{bmatrix}\Phi_{max} & 0 \\ 0 & \Phi_{min}\end{bmatrix}\boldsymbol{R}(\alpha + \beta), \tag{3}$$

where $\boldsymbol{R}(\alpha + \beta)$ is the rotation matrix and $\boldsymbol{R}^{\boldsymbol{T}}$ is transposed or inverse rotation matrix. The strike of the major axis of the ellipse is given by α − β, and in the case of a 2D or 3D/2D Earth, β is zero and the 2-D strike direction is given by α.

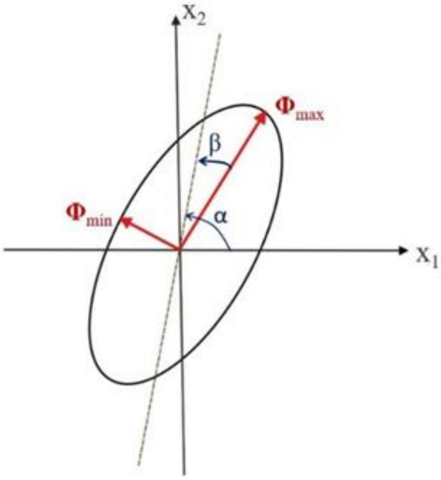

Figure 4: The phase tensor plotted graphically as an ellipse. The maximum and minimum principal axes represented by Φ_{max} and Φ_{min}, respectively. If the phase tensor is non-symmetric, a third coordinate invariant is needed to characterize the tensor: the skew angle, β. The angle α - β, which gives the orientation of the major axis of the ellipse, defines the relationship between the tensor and the observational reference frame (x_1 and x_2); from Caldwell et al. (2004).

For 1-D case, the phase tensor is characterized by a circular shape and a small skew angle. More generally, if the conductivity is both isotropic and 1-D, the radius of the circle will vary with period according to the variation of the conductivity with depth. The radius will increase if the conductivity increases with depth. For a 2-D regional resistivity structure, the phase tensor will be represented by an ellipse and β becomes zero for noise free data and close to zero for a field data. In the presence of 3-D structure, the phase tensor is non-symmetric and the skew angle (β) show large value. Another indication of a 3-D structure is a rapid lateral change of the principal axes direction between sites. Maps of the phase tensor ellipses at different frequency provide a simple way of visualizing lateral changes in the regional conductivity structure at different depths. Such maps will not be influenced by near-surface galvanic effects (Caldwell et al. 2004).

In the Aluto-Langano field, the phase tensor maps plotted at different frequencies reveal the dimensionality of the MT data (Figures 5 and 6). The shapes of the phase tensor and skew angle give an idea of the dimensionality of the subsurface structures. At high frequencies the phase tensor maps indicate small skew angle (-3 < β < 3) as observed in frequencies above 1 Hz (example at 1000 Hz, 137.29 Hz and 11.473 Hz in Figure 5). The shape of the ellipses in generally are circular at higher frequencies and elliptical around 1 Hz implying structures at shallow depths indicating 1-D and 2-D characters (Figures 5 and 6). The phase tensor analysis reveals three-dimensionality below 1 Hz, as deeper structures characterized by a high skew angles (β < -3 and β > 3) and the phase tensors are non-symmetric as indicated below 1 Hz, (example at 0.0800123 and 0.029688 Hz in Figure 6). From the phase tensor analysis, we can see that 3-D inversion is needed to image complex subsurface structures particularly at deeper part of the subsurface.

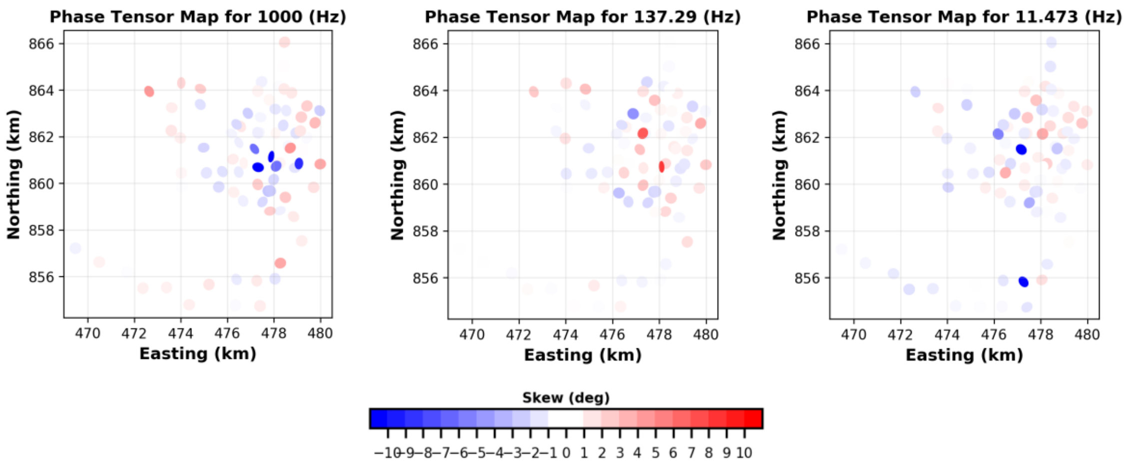

Figure 5: Phase tensor maps at 1000, 137.29 and 11.473 Hz.

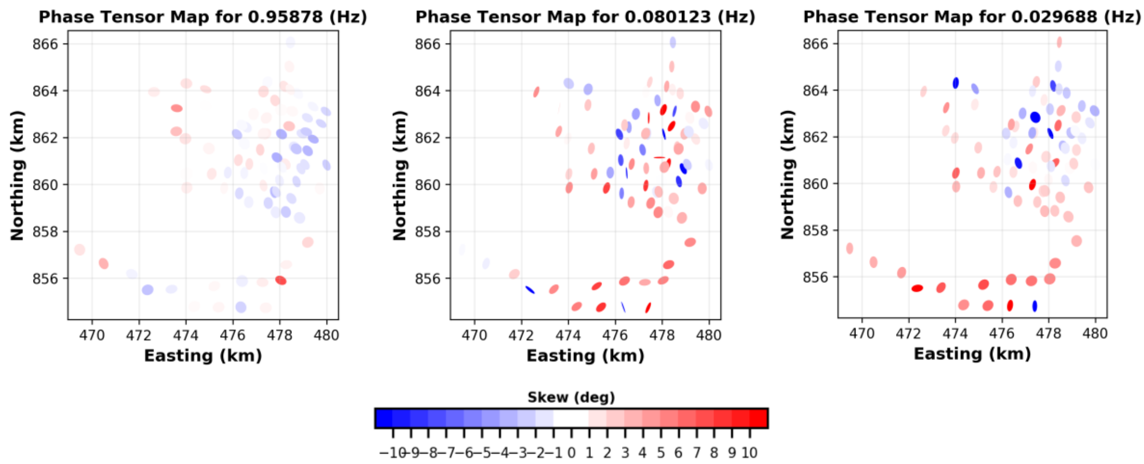

Figure 6: Phase tensor maps at 0.95878, 0.080123 and 0.029688 Hz.

4. 3-D MT Inversion

In recent years, 3-D MT inversion is widely used in geothermal exploration to image subsurface resistivity structures as 1-D and 2-D models are ambiguous and not sufficient to map complex geological structures. We use the 3-D inversion program, ModEM to invert Aluto-Langano MT data (Egbert and Kelbert, 2012; Meqbel, 2009; Kelbert et al., 2014). The 3-D inversion implemented in ModEM code is based on the minimization of the following penalty functional:

$$U(\mathbf{m},\mathbf{d}) = (\mathbf{d}-\mathbf{F}(\mathbf{m}))^T\mathbf{C}_d^{-1}(\mathbf{d}-\mathbf{F}(\mathbf{m})) + \lambda(\mathbf{m}-\mathbf{m_0})^T\mathbf{C}_m^{-1}(\mathbf{m}-\mathbf{m}_0). \quad (4)$$

The first term in the equation represents the data misfit between the measured (**d**) and model response, **F**(**m**). The second term describes the model update between the estimated model (**m**) and initial model ($\mathbf{m_0}$). λ is the regularization parameter, $\mathbf{C}_m$ and $\mathbf{C}_d$ are the model and data covariance's, respectively. In ModEM the penalty function is minimized using the non-linear conjugate gradient (NLCG) method. This algorithm requires a small amount of memory usage as it avoids explicitly computing and storing the Jacobian matrix. The initial model, $\mathbf{m_0}$ is updated iteratively by line search strategy. The 3-D forward problem is based on the finite difference method (FDM).

For the 3-D inversion we used MT data obtained from 65 sites (see Figure 7). The full impedance tensor (Z*xx*, Z*xy*, Z*yx* and Z*yy*) was inverted in the frequency range of 0.011 Hz to 370 Hz for a total of 22 frequencies. The model we employed consisting of 56 x 66 x 49 cells in the x, y and z directions, respectively (181,104 cells in total). In the core the model, the cell dimension in the x and y directions is taken to be 150 x 150 meters. For an accurate model boundary condition, 8 blocks were appended to the mesh boundaries in both directions, and the dimensions of these boundary blocks increased with a factor of 1.3 in all directions. In the vertical direction, a total of 49 layers are used with a surface-layer thickness of 15 meters increasing with a factor of 1.1 for the subsequent layers. Our initial model is a homogeneous half space of 40 Ωm. At the end of the inversion, iteration number 46, the starting RMS reduced to 1.26. Figure 8 shows the distribution of the overall RMS misfit for all sites and for all periods at the end of the inversion.

The 3-D MT inversion result of Aluto-Langano geothermal field reveals three main resistivity structures: a very resistive surface layer with resistivity more than 100 Ωm at shallow depths, a conductive layer underneath the high-resistivity region with a resistivity value of below 10 Ωm and a high resistivity zone at depth, 20 – 60 Ωm. Figure 9 showing resistivity slice maps at different depths. The high-resistivity layer at shallow depths has a thickness of about 170 m. The low conductive zone starts to appear below 170 m at some points in the area and covers most of the area becoming dominant from 200 to around 850 m. Below the conductive zone, resistivity increases gradually with depth as shown in the resistivity slice depth maps.

Figure 10 show resistivity cross-sections extracted from the 3-D MT model along Line A, B and C. The resistivity sections represent the major characteristics of the Aluto-Langano subsurface structures. An elevated high resistivity region beneath conductive layer is observed on the E-W profiles, Line A and B at the western ends. The shallow depth of the area characterized by a resistive layer more than 100 Ωm followed by a conductive zone with a resistivity value below 10 Ωm. The low resistivity layer is strong in the central and northern portion of the area and start to disappear as we move south and west as observed on Line B. Under the low resistivity region, the resistivity increases gradually up to 60 Ωm at the deeper part of the model.

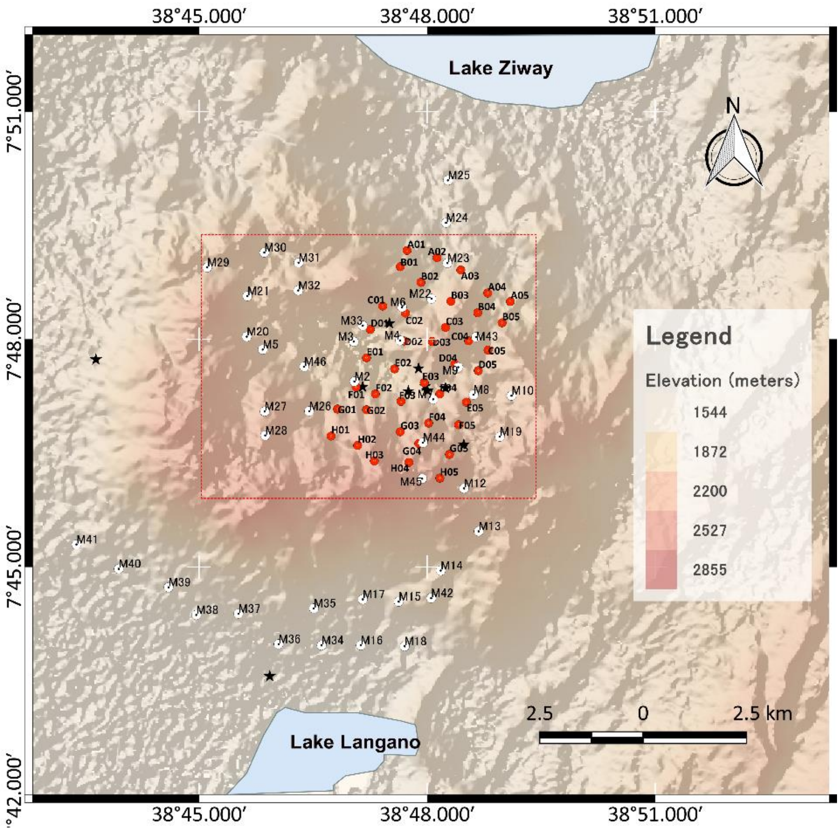

Figure 7: MT stations in Aluto-Langano geothermal field. The red rectangle is the area selected for 3D inversion.

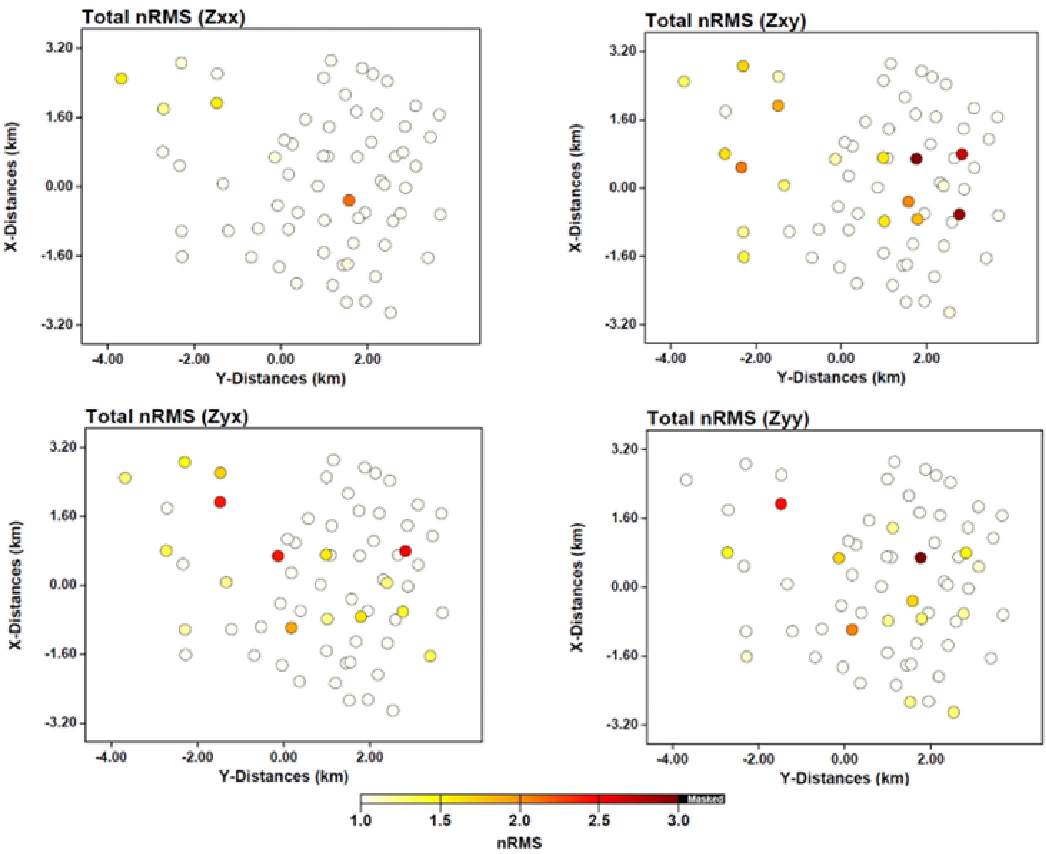

Figure 8: Distribution of RMS misfit for all sites and for all periods at the last iteration.

5. Interpretation of Resistivity Structures

The recovered resistivity model of Aluto-Langano geothermal field from 3-D MT inversion interpreted with the geological information of the area and the conceptual model of high-enthalpy geothermal systems. High-enthalpy geothermal systems have temperatures over 150 ^{0}C and are commonly found in tectonically active regions (Munoz, 2014). In a high-enthalpy geothermal system resistivity distribution is highly dependent on hydrothermal alteration (Ussher et al., 2000; Munoz, 2014). The alteration zones identified in Aluto-Langano geothermal field at recently finished wells, LA-9D and LA-10D are very similar to the conceptual model of high-geothermal systems. In these wells, three alteration zones have been identified below the unaltered zone based on the distribution of alteration minerals (Figure 11A). The *unaltered zone* has a low temperature (< 50 ^{0}C) and has a thickness of 120 m in LA-9D and 130 m in LA-10D wells. The first alteration zone (*Smectite zone*) is characterized by the abundance of Smectite (75 - 150 ^{0}C). The thickness of this region is 380 m in LA-9D and 370 m in LA-10D. The second alteration zone, *Illite/Chlorite zone* (150 – 200 ^{0}C) has a thickness of 520 m and 360 m in LA-9D and LA-10D, respectively. Figure 11A shows, the last alteration zone is the *Illite/chlorite/epidote zone* with temperatures above 200 ^{0}C recognized beneath the *Illite/chlorite zone* in both wells (Selamawit, 2016).

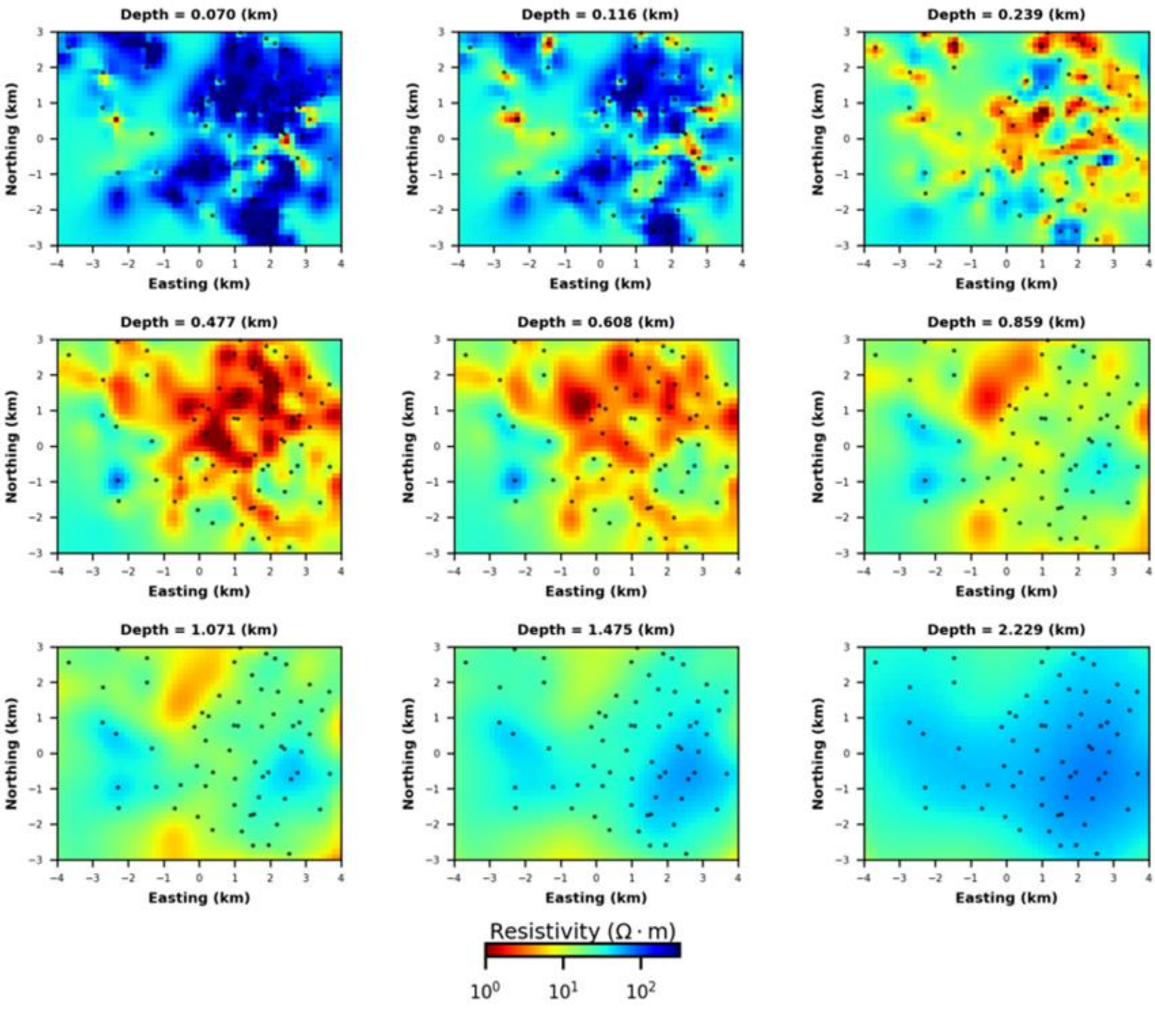

Figure 9: Resistivity slice maps at different depths extracted from the 3-D model.

Above the upflow zone, the conductive clay cap is often elevated near the surface because of the relative increase in higher resistivity minerals in the mixed layer with temperature (Munoz, 2014). The high resistivity zone under the conductive clay cap observed in the 3-D inversion model of Aluto-Langano (Figure 12) have a resistivity between 20 – 60 Ωm. This deep resistive region could be identified as zone of upflow and hottest part of the geothermal field characterized by maximum temperatures more than 300^0C and the presence of propyllitic alteration. In this zone, the most common alteration products include chlorite and epidote. The four deep geothermal wells LA-3, LA-6, LA-9D and LA-10D are drilled into this zone and show a very small temperature gradient for depths below 1000 m, which is a typical feature of upflow zones.

The high-resistivity layer observed at shallow depth is associated with the fresh volcanic rocks in the *unaltered zone* with low temperature (Figures 11 and 12). The argillic alteration zone in high-temperature fields characterized by low resistivity (< 10 Ωm) due to the formation of conductive alteration minerals, particularly Smectite. The resistivity increases gradually (20 - 60 Ωm) at depth beneath the conductive region due to the formation of high-temperature alteration minerals, particularly chlorite and epidote (Figures 11 and 12). The recovered resistivity distribution in Aluto-Langano geothermal field corresponds very well to the conceptual model of a high-enthalpy geothermal system as an increase in resistivity below a highly conductive surficial layer (clay cap), reflecting an increase in temperature with depth, is a common signature of high-temperature geothermal systems (Munoz 2014).

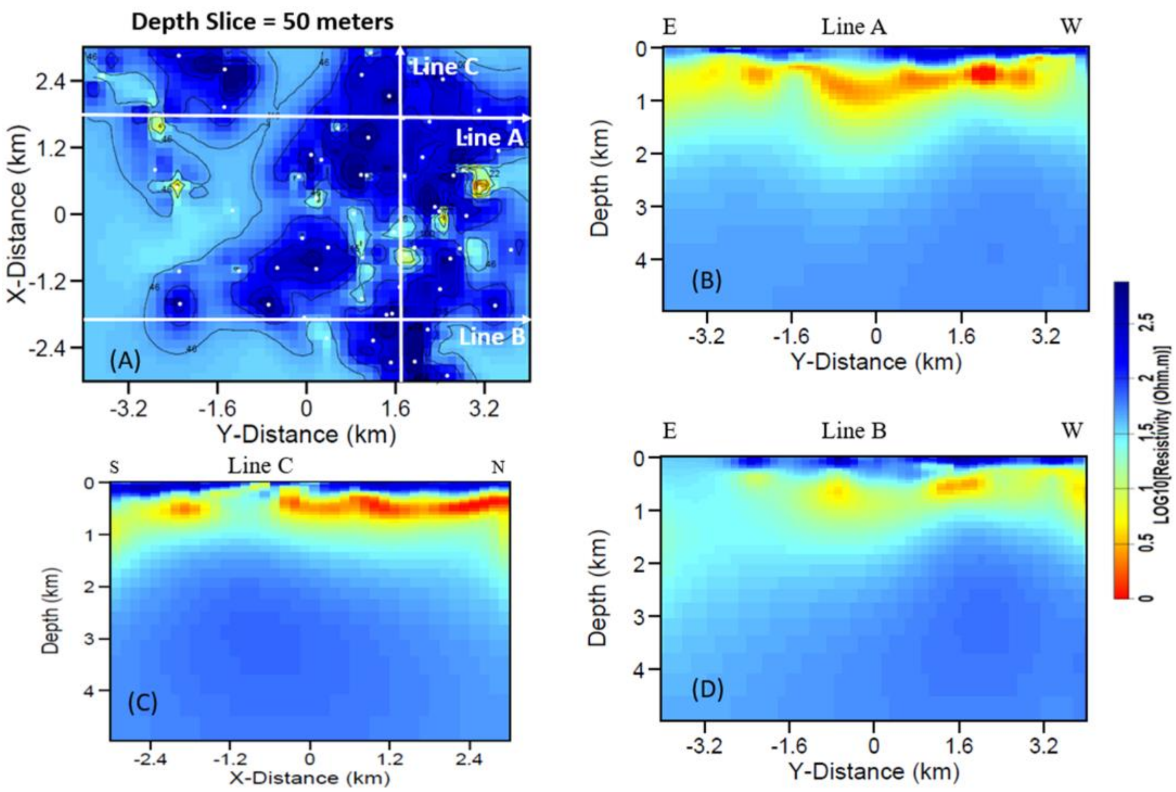

Figure 10: Resistivity cross-sections extracted from the 3-D inversion resistivity model along E-W and N-S directions. (A) Depth slice map at 50m from the ground. MT stations are indicated as white dots. (B) Resistivity cross section extracted in E-W directions along Line A. (C) Resistivity cross section extracted in N-S directions along Line C. (D) Resistivity cross section extracted in E-W directions along Line B.

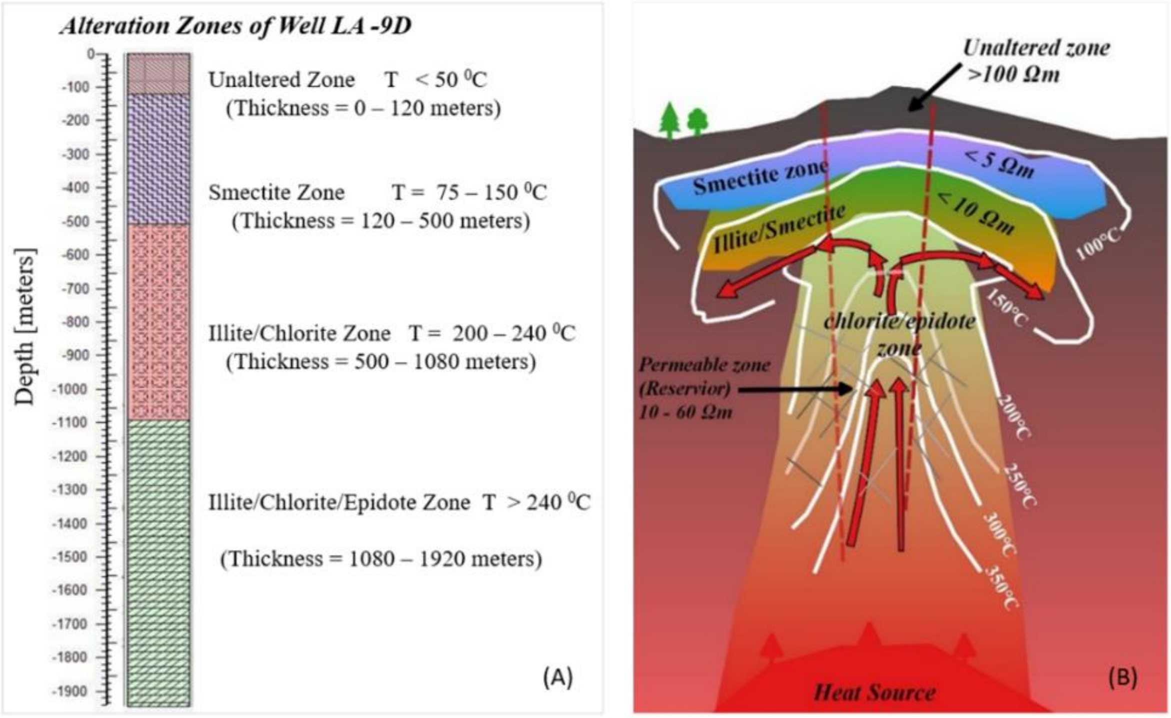

Figure 11: (A) Temperature and alteration zones in LA-9D well (Modified from Selamawit, 2016). (B) A conceptual model of a high-enthalpy geothermal system (Modified from Johnston et al., 1992 and Cumming and Mackie, 2007; Samrock et al., 2016; Cherkose and Mizunaga, 2018).

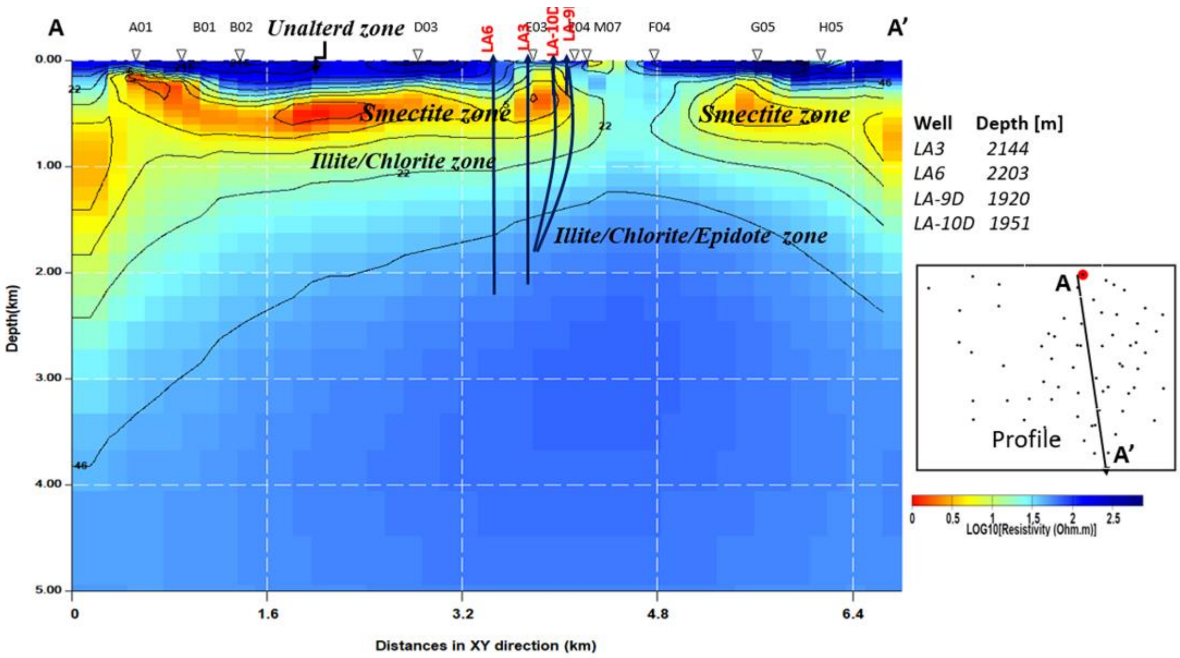

Figure 12: Resistivity cross-section extracted from the 3-D model interpreted based on drilling information and the conceptual model of high-enthalpy geothermal systems. LA3, LA6, LA-9D and LA-10D are deep geothermal wells drilled into the upflow zone.

6. Conclusions

MT data from two surveys conducted in 2009 and 2012 for the Aluto-Langano geothermal field were evaluated and inverted in three dimensions using ModEM program. The recovered 3-D resistivity model revealed structures that corresponds very well to the conceptual model for high-enthalpy volcanic geothermal systems. The low resistivity anomaly associated with clay cap alteration mineralogy is clearly imaged over a higher resistivity high-temperature reservoir. This conductive clay cap is overlying the resistive propylitic upflow zone as confirmed by the geothermal wells in the area.

However, a low resistivity zone that would indicate the presence of a heat source below the resistive upflow zone is absent in the recovered 3-D resistivity model. The resistivity shows a gradual increase beneath the conductive layer indicating no sign of a distinct resistivity structure at greater depths under the resistive propylitic upflow zone. There may be ways to remedy this shortcoming by incorporating longer period data within the inversion process at the expense of larger grids and greater computational time.

The central and southern portions of the area that show uplifted high resistivity zones detected underneath the conductive layer, can be seen as promising zones for drilling targets for production wells. However, the suggested locations should be investigated further following an integrated approach, by including other geophysical, geological and geochemical surveys.

Acknowledgments

The authors would like to thank West JEC and Dr. Friedemann Samrock from ETH, Zurich for providing the MT data for this study. We sincerely acknowledge the Geological Survey of Ethiopia for the permission to use the MT data from Aluto-Langano for this paper. Special thanks to Mr. Solomon Kebede, Head of Geothermal Resource Exploration and Evaluation Directorate at the Geological Survey of Ethiopia, for his assistance. We also thank Gary Egbert, Anna Kelbert and Naser Meqbel for the ModEM program. Finally, we would like to acknowledge the support of Japan International Cooperation Agency (JICA) for their contribution to the successful accomplishment of the study. We would particularly like to thank Mayumi Hayashi, JICA expert in Ethiopia for her assistance.

REFERENCES

Abebe.T, Pasqua. C, Kebede. S. (2016). Aluto-Langano geothermal field (Ethiopia), proposal of a new geo-golcanological model by combining the existing data with modern studies., *Proceedings, 6th African Rift Geothermal Conference Addis Ababa, Ethiopia November 2016*.

Caldwell, G., C. Pearson, H. Zayadi (1986). Resistivity of rocks in geothermal systems: a laboratory study, *Proceedings 8th NZ geothermal workshop*, 227– 231.

Caldwell, T.G., Bibby, H.M., Brown, C. (2004). The magnetotelluric phase tensor, *Geophys J Int*, **158**, 457–469.

Cherkose, B.A and H. Mizunaga. (2018). Resistivity imaging of Aluto-Langano geothermal field using 3-D magnetotelluric inversion., *Journal of African Earth Sciences*, **139**, 307-318.

Cumming W., and Mackie, R. (2007). 3D MT resistivity imaging for geothermal resource assessment and environmental mitigation at the glass mountain KGRA, California, *GRC Transactions*, **31**, 331–334.

Egbert G.D., Kelbert, A. (2012). Computational recipes for electromagnetic inverse problems, *Geophys. J. Int*., **189**, 251–267.

Ernst & Young, JETRO, West JEC (2010). Study on Geothermal Power Development project in the Aluto Lanagno Field, Ethiopia, Final Report.

Gebregzabher, Z. (1986). Hydrothermal alteration minerals in Aluto Langano geothermal wells, Ethiopia, *Geothermics*, **15**, 735–740.

Gianelli, G., and Teklemariam, M. (1993). Water-rock interaction processes in the Aluto-Langano geothermal field (Ethiopia), *J. Volcanol. Geotherm*., Res., **56**, 429–445.

Hersir, G.P., and Björnsson, A., (1991). Geophysical exploration for geothermal resources. Principles and application., UNU-GTP, Iceland.

Hutchison. W, Pyle.D.M., Mather. T.A., Yirga. G, Biggs. J, Cohen. B.E, Barford. D.N, Lwei. E. (2016). The eruptive history and magmatic evolution of Aluto volcano: new insights into silicic peralkaline volcanism in the Ethiopian rift., *Journal of Volcanology and Geothermal Research*, **328**, 9–33.

Johnston, J., Pellerin, L., Hohmann, G. (1992). Evaluation of electromagnetic methods for geothermal reservoir detection, *Transactions-Geothermal Resources Council*, **16**, 241–245.

Kelbert, A., N.M.Meqbel, G.D. Egbert and K. Tandon (2014). ModEM: A modular system for inversion of electromagnetic geophysical data, *Comp. Geosci*., **66**, 40-53.

Martí, A., P. Queralt, J. Ledo, C. Farquharson, (2010). Dimensionality imprint of electrical anisotropy in magnetotelluric responses, *Physics of the Earth and Planetary Interiors*, **182**, 139–151.

Meqbel, N.M.M. (2009). The Electrical Conductivity Structure of the Dead Sea Basin Derived from 2D and 3D Inversion of Magnetotelluric Data, Ph.D. thesis.

Munoz, G. (2014). Exploring for geothermal resources with electromagnetic methods, *Surv. Geophys*., **35**, 101–122.

Pellerin L, Johnston JM, Hohmann GW (1996). A numerical evaluation of electromagnetic methods in geothermal exploration. *Geophysics* **61**, 121–130

Samrock, F., A. Kuvshinov, J. Bakker, A. Jackson, and S. Fisseha. (2015). 3-D analysis and interpretation of magnetotelluric data from the Aluto-Langano geothermal field, Ethiopia, *Geophys. J. Int*., **202**, 1923–1948.

Selamawit, W., S. (2016). Subsurface Geology and Hydrothermal Alteration of Wells LA-9D and LA-10D of Aluto-Langano geothermal field, Ethiopia. *Proceedings, 6th African Rift Geothermal Conference Addis Ababa, Ethiopia, 2nd -4th, November 2016*.

Ussher, G., R. Harvey, C. Johnstone, E. Anderson (2000). Understanding the resistivities observed in geothermal systems, *Proceedings of World Geothermal Congress*, 1915–1920.